

2019 EHP Award G19AP00024

Defining the boundaries of the Eastern Tennessee Seismic Zone by understanding its geodynamic and seismotectonic origin

Will Levandowski*

Boulder Geophysics

* Now at TetraTech, Inc.

1100 S. McCaslin Blvd, Superior, CO 80027

(303)-448-7412

BoulderGeophysics@gmail.com; will.levandowski@tetrattech.com

Grant Time Period: January 1, 2019-December 31, 2019

ACKNOWLEDGMENT OF SUPPORT: This material is based upon work supported by the U.S. Geological Survey under Grant no. G19AP00024.

DISCLAIMER: The views and conclusions contained in this document are those of the authors and should not be interpreted as representing the opinions or policies of the U.S. Geological Survey. Mention of trade names or commercial products does not constitute their endorsement by the U.S. Geological Survey

ABSTRACT

Earthquake rates in the Eastern Tennessee Seismic Zone (ETSZ) are 5–10 times higher than the central and eastern United States (CEUS) average, second only to the New Madrid area. Known fault sources are absent in the ETSZ, so the National Seismic Hazard Model (NSHM) bases estimates solely on moderate-magnitude historical seismicity rates, which are also treated differently in the ETSZ than in its surroundings. Nevertheless, the cause of elevated ETSZ earthquake rates is unknown, and—because intraplate earthquakes may cluster in space and time—it is unclear whether and by how much long-term ETSZ hazard is greater than the rest of the southeastern US (SEUS). Moreover, without knowing what property or process concentrates earthquakes in the ETSZ, it is not possible to determine the extent of the high-hazard/special-treatment zone. Indeed, the ETSZ lies along a major Proterozoic suture zone that runs ~1,600 km NNE from Alabama to southern New England, yet it is the only notably active portion over the past 200 years. In addition to the 3 million people within the region loosely defined by historical seismicity, up to 10 million more could be at risk if the active seismic zone extends an additional ~75 km to Atlanta, Nashville, or Birmingham, or 150 km to Charlotte.

This project aims to clarify the spatial extent of SEUS hazard by determining what causes concentrated seismicity in the ETSZ and mapping where else these same properties or processes are present in the SEUS. First, crustal stress across the CEUS is mapped with focal mechanism inversions, revealing a cornerstone constraint on the cause of ETSZ seismicity: Everywhere else in the continental SEUS displays the ENE–WSW compression expected from plate tectonics, but the ETSZ is in a unique state of oblique extension. A local source of tension greater in magnitude than transmitted plate-boundary stress is required. Identifying this stressor and mapping where it acts may demarcate the true extent of the ETSZ. Previous studies have identified anomalous middle/lower crust in the ETSZ, and other work has examined similar features along other multiply reactivated Proterozoic sutures, finding that alteration-related density anomalies are capable of generating sufficient (gravity-derived) stress to control earthquake locations. To compute 3D gravity-derived stress, surface wave dispersion and ellipticity, receiver functions, gravity, heat flow, and topography are jointly inverted to generate a 3D lithospheric density model of the SEUS, which is then passed to finite-element simulations of 3D stress. The most buoyant lower crust in the SEUS appears beneath the ETSZ, and this material generates anomalous NW–SE tension. The gravity-derived stress field sums with an unknown tectonic stress field assumed to be broadly uniform across the CEUS, which is determined by optimizing fit between the summed 3D stress field and the results of focal mechanism stress inversions.

The final estimate of total crustal stress reveals the spatial extent of the ETSZ as a seismotectonic entity, the expected long-term seismicity rates in the ETSZ relative to surroundings, and the locations of known or yet-unknown foci of elevated long-term stress. An area of modeled buoyancy-driven oblique extension runs along the southern Appalachians from northern Alabama to southern Pennsylvania, yet the peak deviatoric stress occurs in the ETSZ and western North Carolina. In this area, deviatoric stress magnitude is ~5 times the regional average, roughly accounting for the 5-fold greater seismicity rate in the ETSZ without invoking low-viscosity material or other sources of weakness. In addition to the ETSZ, long-term net deviatoric stress is highest near New Madrid and is elevated along the Virginia/West Virginia Appalachians and some portions of the Midcontinent Rift. Mismatches between historical seismicity and modeled stress levels could reflect the impacts of surface processes, shortcomings of the modeling approach, more complex boundary conditions, variable stress due to asthenospheric flow, rheologic variations including high/low viscosity lithospheric roots, influences of material below 150 km, or simply our incomplete record of the full seismic cycle across the CEUS.

REPORT

1. INTRODUCTION

Earthquake rates are 5–10 times higher in the ETSZ than the CEUS average, second only to the New Madrid region. With 2.4 $M_L \geq 3$ earthquakes per year and a Gutenberg-Richter b-value of ~ 0.94 [Bockholt *et al.*, 2015], a $M_L 6$ event is anticipated every ~ 275 years, although—in contrast to New Madrid—no large historical shock is known.

Globally, proposed explanations for locally elevated seismicity rates in intraplate settings like the ETSZ can be grouped into four categories. Since intraplate aftershock sequences may persist for 1000 years or more [Stein and Liu, 2009], the simplest scenario is that modern earthquakes are principally the legacy of a major but unknown prehistoric event rather than the result of locally elevated long-term strain accrual [e.g., Ebel *et al.*, 2000]. Nevertheless, epidemic-type aftershock sequence models in the ETSZ demonstrate that only ~ 0.04 of the 2.4 annual $M_L \geq 3$ earthquakes (with a maximum of 0.21 per year at 95% confidence) are readily ascribed to such a phantom event [Levandowski and Powell, 2018], leaving three tenable explanations.

In contrast to aftershocks, earthquakes in the three remaining situations chiefly release long-term strain, yet they have different implications for long-term hazard. Intraplate seismicity often clusters in space and time [e.g., Clark *et al.*, 2012]. Therefore, ETSZ events could represent a naturally active phase of strain release in what is a broadly uniform long-term stress(ing)—and thus strain-rate—field. If so, seismic hazard need not be stationary, and damaging earthquakes may be equally likely in and outside of the ETSZ [e.g., Stein and Liu, 2009]. The third class of explanations invokes weakness, such as through low-viscosity ductile lithosphere, low-friction brittle faults, or characteristically low stress-drop events. Under uniform stressing, these areas may experience higher strain rates, higher earthquake rates, or both. In this case, future seismicity rates would remain higher in the ETSZ than elsewhere, and past events may outline the most likely locations of future impactful earthquakes. Finally, stress(ing) could be distinct in seismically active regions: Localized sources of stress sum (in a tensor sense) with regional stress(ing), perturbing the net stress state, and potentially elevating overall deviatoric loading. As in weak zones, seismic hazard would again be roughly stationary over time.

The crustal stress field may shed light on the seismotectonics of the ETSZ and in so doing help to differentiate among these three remaining possibilities. Naturally periodic strain release and earthquakes in weak zones should reflect the long-term stress(ing) field; if stress(ing) is uniform across the CEUS, the ETSZ stress field should be indistinguishable from its surroundings. By contrast, a distinct state of stress in the ETSZ could not readily be explained by weak material or temporal clustering but would instead suggest a localized source of stress. Although a distinct net stress state does not require constructive interference between the local and regional stressors, elevated net deviatoric stress would also explain the focusing of seismicity.

Here, the crustal stress field is mapped using inversions of existing and newly compiled focal mechanisms, and these inversions demonstrate an oblique extensional strain regime in the ETSZ that is significantly different from the reverse, reverse-oblique, and strike-slip faulting elsewhere in the CEUS. To understand the origin of the observed stress variations and to delineate whether similar conditions exist elsewhere in the CEUS, a 3D forward model of lithospheric stress is developed by mapping crustal and upper mantle density, computing the associated gravitational (i.e., body force-derived) stress field, and solving for the single regional stress field that—when summed with gravitational stress—optimally fits the observed stress state. In turn, the magnitudes and principal directions of this net stress serve as proxies for variations in expected long-term strain rate and deformation style across the CEUS.

2. GEOLOGIC AND GEOPHYSICAL SETTING

The ETSZ is defined by a ~250-km NNE–SSW band of epicenters that parallels the grain of the southern Appalachians (Figure 1A,B). Nevertheless, earthquakes are not associated with Paleozoic faults or overthrust units but occur within Grenville-age basement [e.g., *Powell et al.*, 2014]. Unlike many other intraplate seismic zones [e.g., Johnston and Kanter, 1990], including New Madrid, the ETSZ is not associated with rifted lithosphere. The area of most concentrated seismicity is, however, tightly bounded along its northwest by a major Proterozoic strike-slip boundary [*Powell and Thomas*, 2016; *Steltenpohl et al.*, 2010]. This basement feature manifests as the New York-Alabama Lineament (NYAL), a 1,600 km-long magnetic anomaly associated with Bouguer gravity lows [*King and Zietz*, 1978]. Seismicity mainly occurs in comparatively non-magnetic basement SE of the shear, within a negative Bouguer and isostatic residual gravity anomaly (Figure 1B).

Shear along the NYAL demonstrably strained adjacent crust and mantle lithosphere, but this ancient deformation is not a sufficient condition for modern seismicity: The ETSZ is the only location along the NYAL that is anomalously seismogenic. Strain in the mantle lithosphere manifests in NYAL-parallel SKS fast directions [*Wagner et al.*, 2012; *Long et al.* 2016] and *Pn* anisotropy [*Buehler and Shearer*, 2017] both within the ETSZ and elsewhere along strike. Crustal modification is suggested by low group-velocity crust (to at least 15s period) in the ETSZ that is flanked by higher-velocity regions [*Brandmayr et al.*, 2016; *Bockholt*, 2014], and by deeper magnetic basement along the NYAL (6–12 km) than its surroundings (0–4 km) [*Brandmayr and Vlahovic*, 2016]. As with NE-SW fast directions, however, deep magnetic basement and surface wave anomalies continue NE and SW along strike beyond the epicentral region into quiescent areas. The lack of earthquakes elsewhere implies that the inheritance of the lithospheric-scale shear zone is insufficient to explain earthquake localization in the ETSZ. Additionally, upper mantle thinning/warming/weakening along the NYAL generally or in the ETSZ specifically is not supported geophysically: Both teleseismic P-wave tomography [*Biryol et al.*, 2016] and long-period surface wave dispersion [*Shen and Ritzwoller*, 2016; *Pollitz and Mooney*, 2015; *Wagner et al.*, 2018] image higher-velocity upper mantle beneath the ETSZ than the adjacent and largely aseismic Piedmont and Triassic basins, and ETSZ heat flow is modestly low relative to surroundings (~35 vs. ~45 mW/m²) [*Blackwell et al.*, 2011]. All of these observations challenge a direct, causal link of current seismicity with the prominent Proterozoic structures and deformation.

The ETSZ is associated with spatially limited crustal structure that may play an important role in the localization of earthquake activity. Modern earthquakes do not occur on the major NE–SW-trending structures, however (Figure 1C). Instead, most focal planes and epicentral alignments illuminate high-angle *en echelon* N–S and NNE–SSW-striking faults [*Chapman et al.*, 1997]. The NYAL bends southward near 35°N (the Tennessee/Georgia border; Figure 1A,B). A set of relay structures in the brittle crust would have been necessary to accommodate this bend in the Proterozoic shear system, creating a zone of “concentrated crustal deformation” [coined by *Thomas and Powell*, 2017] and right-stepping fault sets at the modern ETSZ. Sinistral NYAL motion documented in apparent polar wander curves [*D’Agrella-Filho et al.*, 2008] implies that these secondary faults initiated as high-angle releasing structures. There, local earthquake tomography images a near-vertical low-*Vp* and -*Vs* zone to at least 24 km depth; jointly considering absolute velocities, gravity, and magnetic signatures, *Powell et al.* [2014] suggest mylonitized crust in this heavily deformed relay zone. Additionally, the Moho in the southern

ETSZ—near the bend in the NYAL—appears gradational or is absent on receiver functions, which has been interpreted to reflect lower crustal delamination, serpentinization, or other localized modification [Graw *et al.*, 2015]. Whereas the NYAL as a whole cannot be directly related to focused ET SZ seismicity, these spatially limited crustal features related to large-scale Proterozoic shear-zone geometry may influence modern deformation.

3. CRUSTAL STRESS

3.1 PREVIOUS WORK

3.1.1. CEUS

The maximum horizontal compressive stress direction (σ_{Hmax}) across the CEUS is broadly ENE–WSW [e.g., Sbar and Sykes, 1973], consistent across thousands of km (Figure 1A). This long-wavelength σ_{Hmax} parallels the ENE–WSW compressional traction applied by Mid-Atlantic Ridge push and the compression expected from absolute plate motion (via asthenospheric drag traction) [e.g., Zoback and Zoback, 1980]. These observations were taken as early evidence that plate tectonic processes control intraplate stress and have led to the conventional understanding [e.g., Zoback, 1992] that the stress field in the CEUS is more or less homogeneous, driven by global tectonic processes.

The most robust constraints on σ_{Hmax} , especially in low-seismicity regions such as the CEUS, come from wellbore breakouts. These and other *in-situ* indicators, however, typically contain little information outside of the horizontal plane and therefore do not demonstrate whether a region is undergoing net horizontal shortening, simple shear, or net horizontal extension (deformation styles typified by thrust/reverse, strike-slip, and normal faulting, respectively). By contrast, earthquake focal mechanisms directly record faulting style, albeit with weak constraint on stress directions [e.g., McKenzie, 1969].

Over the past decades, continued routine monitoring, evolving seismic techniques, and expanded network coverage have increasingly availed focal mechanism solutions in the CEUS. Consistent with the canon of ENE–WSW horizontal shortening parallel to—and inferred to result from—plate boundary and/or basal tractions, most CEUS earthquakes record reverse, reverse-oblique, or strike-slip motion and have near-horizontal maximal shortening axes (P-axes) that trend, on average, ENE–WSW (Figures 1A,2A).

3.1.2. ET SZ

Horizontal principal stress directions in the ET SZ conform to the CEUS-wide pattern of ENE–WSW σ_{Hmax} (Figure 1A,D). Five sets of borehole breakouts NNE and ESE of the ET SZ proper [compiled by Heidbach *et al.*, 2016] have an average σ_{Hmax} of N58°E. Similarly, the 26 first-motion focal mechanisms of Chapman *et al.* [1997] are dominated by ENE–WSW P-axes, and formal inversion of these mechanisms [Mazzotti and Townend, 2010] yields a best-fit σ_{Hmax} of N54°E. Because these unremarkable principal stress directions give no reason to question conventional understanding of a plate-scale tectonically-driven stress field, ET SZ seismicity has mainly been interpreted as simple reactivation of inherited faults [e.g., Powell *et al.*, 1994; Chapman *et al.*, 1997; Mazzotti and Townend, 2010], by implication in a uniform stress(ing) field.

Details of earlier studies and recent work, however, hint at an anomalous deformation style in the ET SZ (Figure 1C–D, 2A–B). Net horizontal shortening—reverse, reverse-oblique, and strike-slip faulting—characterizes CEUS focal mechanisms (Figures 1A, 2A). By contrast, negative rakes in nearly all (22 of 26) events studied by Chapman *et al.* [1997] demonstrate a

consistent component of net ESE–WNW extension (Figures 1A, 1D, 2B). Inversion of these mechanisms [Mazzotti and Townend, 2010] shows no statistically significant difference between the magnitude of σ_{Hmax} and $\sigma_{vertical}$, requiring roughly equal parts extension and simple shear. (Mazzotti and Townend do not explicitly state the uncertainties for this stress ratio, but confidence intervals of σ_{Hmax} and $\sigma_{vertical}$ are plotted, and they overlap.) More recently, Cooley [2014] derived an additional 26 focal mechanisms, finding substantial extension, especially in the southern ETSZ. This extension defies explanation as simply the result of plate-boundary tractions, which are compressional. The present work quantifies the state of stress in the ETSZ, and then to compare crustal stress in the ETSZ with that in other parts of the CEUS.

3.2 NEW STRESS INVERSIONS

3.2.1. Methodology

The inversion of focal mechanisms for the crustal stress tensor is well established and stems from the axiom that coseismic slip parallels the shear traction resolved on the fault plane [e.g., Angelier, 1973]. The latter depends linearly on the orientation of the fault and on the 3D stress tensor; this linear system quickly becomes overdetermined with multiple slip observations from faults of different orientations. Inverting this system yields the normalized stress tensor that minimizes the angular misfit between the shear traction on the fault planes and the slip vectors. We use an iterative inversion methodology [using code modified from Vavryčuk, 2014] that selects between the two nodal planes for a given mechanism based on their instability; the less stable nodal plane is the one that is better oriented for shear faulting. Since stability depends on friction, each inversion (see below) selects a random frictional coefficient from a uniform distribution between 0.3 and 1 to account for uncertainty with respect to friction in focal plane selection.

The normalized stress tensor can be fully described in terms of the directions and relative magnitudes S of the three principal stresses. The stress ratio Φ is given as:

$$\Phi = (S_2 - S_3) / (S_1 - S_3) \quad (1)$$

Simpson [1997] combined Φ with the style of faulting (normal/strike-slip/reverse, as defined by principal axis plunges [Zoback, 1992]) to describe the style of deformation as a quantity $A\Phi$:

$$A\Phi = (n + 0.5) + (-1)^n(\phi - 0.5), \quad (2)$$

with $n=0$ for normal faulting, 1 for strike-slip, and 2 for thrust.

Consequently, $A\Phi$ defines a continuum from 0 (radial extension) to 3 (radial contraction), passing through: uniaxial extension/pure normal faulting, $A\Phi=0.5$; oblique extension, $A\Phi=1.0$; horizontal shear/strike-slip, $A\Phi=1.5$; oblique contraction, $A\Phi=2.0$, and uniaxial contraction/pure thrust, $A\Phi=2.5$.

Thus, stress inversions quantify the best-fitting deformation style ($A\Phi$) and principal stress directions. Variations in stress can be discussed in terms of differences in $A\Phi$ and σ_{Hmax} . By contrast, most *in-situ* stress indicators such as borehole breakouts are typically only meaningfully sensitive to σ_{Hmax} .

3.2.2. Dataset and inversion details

Most (52 of the 62) ETSZ focal mechanisms are derived from first motions. The 26 mechanisms of Chapman *et al.* [1997] are based on P-wave first motions, and 26 additional events using P and SH polarities studied by Cooley [2014] are reanalyzed for this study; an average of 22 polarities are available per event. Strike, dip, and rake of the remaining 10 events

are constrained by moment tensors derived from waveform fitting [Herrmann, 2019; USGS, 2019].

First-motion focal mechanisms are non-unique. With a finite number of first-motion constraints, many strike/dip/rake combinations may exactly reproduce all of the polarities. Alternatively, there may be no combination that recovers all polarities but many solutions that only produce one error. All of these solutions fit their respective data equally well; all minimum-polarity-mismatch solutions for each event—18, on average—are retained for use in inversions. The simplest way to embrace this non-uniqueness is to randomly select a solution for each event and invert these 62 mechanisms for the best-fit tensor (iteratively choosing the less stable nodal plane for each mechanism). Repeating this process 100 times for 100 random combinations of acceptable mechanisms, solving for 100 tensors, constrains uncertainties (Figure S1).

At this point, however, the non-uniqueness of focal mechanism solution can be advantageous: Since the fundamental underlying assumption of stress inversions is that all events to be inverted occurred in a homogenous stress field, the best-fitting mechanism for a given event can be constrained by the others. Once the randomly selected mechanisms are inverted for an initial estimate of the stress tensor, the angular misfit between the attendant shear traction on the reported fault planes and reported slip vectors can be calculated. (For reference, the mean misfit across the 100 initial inversions averages 32° , and 45° has been suggested as a threshold of effectively homogenous stress [Hardebeck, 2012]). The algorithm therefore revisits each event and calculates the misfit for all of its acceptable mechanisms, selects the best-fitting, identifies its less stable nodal plane, and inverts the updated set of 62 mechanisms. This calculation-selection-inversion process then iterates (here, 50 iterations per inversion) to compute one best-fitting stress tensor and to determine the associated best-fitting focal mechanisms. To account for uncertainty with respect to the initial selection of focal mechanisms, this process repeats 100 times: Each iterative inversion randomly chooses one mechanism for each event, selects the less stable of the two nodal planes given the friction randomly chosen in this inversion, inverts for an initial estimate of the stress tensor, and then iteratively selects the best-fitting focal mechanism for each event. Across the 100 iterative inversions, average mean misfit is roughly halved, from 32° in the initial models to 17° once the best-fitting mechanisms for each event have been iteratively identified.

On a methodological side note, this study finds that the choice of optimal mechanism for each event is often stable with respect to the initial model and friction: Approximately half the events ultimately select the same mechanism in >95% of the inversions. Figure S1 compares the random-mechanism inversions and iterative inversions. The results are similar, and the iterative approach is more precise. This small methodological tweak warrants future consideration in other situations dominated by first-motion mechanisms that may be individually poorly constrained.

Regional stress in the CEUS is determined using mechanisms from the region shown in Figure 1B, which are nearly all constrained by moment tensor inversions [Herrmann, 2019; USGS, 2019]. The vast majority of events north of this area, from $\sim 43^\circ\text{N}$ northward, display thrust mechanisms (Figure 1A) so would accentuate the differences in $A\Phi$ with the ETSZ (Figure S2). Because coseismic and postseismic processes perturb the stress field—such that aftershocks can display a distinct stress state [e.g., Martinez-Garzón *et al.*, 2018]—events near the 2011 M5.8 Mineral, Virginia earthquake are excluded. Retaining these events also increases $A\Phi$ estimates for the CEUS (Figure S2). Finally, stress near New Madrid is anomalous, featuring a slight clockwise rotation of $\sigma_{H\text{max}}$ and greater propensity for thrust faulting (higher $A\Phi$) than

adjacent areas [e.g., *Grana and Richardson*, 1996; *Hurd and Zoback*, 2012; *Levandowski et al.*, 2016; 2018]. Excluding these three regions therefore generates conservatively low estimates of regional $A\Phi$ in the CEUS. The retained CEUS dataset comprises 38 events from north of the ETSZ (for discussion, termed the Ohio River Basin, ORB), 65 to the east of the ETSZ in and near South Carolina, and 28 mechanisms from northeast of the ETSZ along the Mid-Atlantic region, excluding from central Virginia. These 130 mechanisms are inverted together and in three separate inversions to constrain the background stress field and spatial patterns therein, respectively.

Strike/dip/rake uncertainty is not explicitly calculated with waveform modeling-based moment tensors. Empirically, mechanisms derived using two independent approaches [*Herrmann et al.*, 2011] agree within 15° for 95% of events [*Levandowski et al.*, 2018], so we take a normal distribution with 7.5° standard deviation as characteristic uncertainty. In each inversion (in the ETSZ and outside), such noise is added to the reported 3D slip vector. Moment tensor-based mechanisms are additionally jackknife-resampled: Each inversion ignores the square root of the number of total events (e.g., in the ORB, 6 of the 38 events are discarded in each inversion).

3.2.3. Results: Anomalous extension in the ETSZ

Although most previous work noted the consistent σ_{Hmax} across the CEUS and inferred a rather uniform state of stress, the recent growth in available earthquake focal mechanisms has allowed more thorough quantification of the full state of stress. As previously noted, σ_{Hmax} is similar in the ETSZ ($N55E \pm 1^\circ$) and greater CEUS ($N62E \pm 2^\circ$) (Figure 2C–D). There is a modest range in the CEUS subregions examined, from $N56E \pm 1^\circ$ in the ORB to $N72E \pm 3^\circ$ in the Mid-Atlantic States (Figure S2). The CEUS is dominated by contraction with secondary shear: $A\Phi = 2.22 \pm 0.02$ (Figure 2C). Taking a more granular view, contraction along the Atlantic Margin ($A\Phi = 2.52 \pm 0.05$ in South Carolina, 2.39 ± 0.06 in the Mid-Atlantic) transitions to dominant reverse-oblique faulting ($A\Phi = 1.86 \pm 0.03$) in the ORB (Figure S2).

The strain regime in the ETSZ is different from anywhere else in the eastern United States. Horizontal extension with a substantial shear component dominates: $A\Phi = 0.90 \pm 0.02$ (Figure 2D). This extensional state differs from oblique contraction in the adjacent ORB by 26 standard deviations and from the reverse-oblique faulting of the CEUS as a whole by 1,650 standard deviations.

4. POSSIBLE CAUSES OF UNIQUE STRESS IN THE ETSZ

Above, four classes of explanation for elevated earthquake rates were enumerated. These hypotheses invoke differing origins of the strain ultimately released by ongoing earthquakes. First, aftershocks of a major but prehistoric earthquake could increase seismicity rates, with the strain released a combination of stored tectonic energy and post-seismic adjustments. Nevertheless, ETSZ-specific aftershock sequence modeling [*Levandowski and Powell*, 2018] demonstrates that—to 95% confidence—less than 10% of ongoing earthquakes may be the result of such a phantom event, likely far fewer. Second, intraplate seismicity can cluster in space and time, such that ETSZ earthquake rates represent a comparatively active phase of naturally periodic release of long-term strain. Taken alone, this hypothesis implies that the ETSZ is accommodating its share of North America’s overall intraplate strain budget and simply releases stored elastic energy episodically. Third, having endured a rich history of deformation, the ETSZ lithosphere may have been weakened in any of numerous ways. Under uniform plate-boundary

or basal loading, strain and/or earthquake rates would be higher in the ETSZ than elsewhere. As such, the ETSZ would again accommodate its share of North America's strain budget, even if its share is disproportionate because of inherited weakness.

The ETSZ is not simply accommodating its share of North America's strain budget, however. The ETSZ is straining in quite a different way from the rest of eastern North America. The long-term, long-wavelength, tectonic strain that causes reverse, reverse-oblique, and strike-slip faulting (horizontal contraction) across the CEUS is not simply stored elastically and released by the normal and oblique-normal earthquakes (horizontal extension) in the ETSZ. Naturally periodic seismicity or zones of weakness alone therefore are not sufficient to explain ongoing ETSZ seismicity, though they may play a role in overall seismicity rates.

The fourth class of explanation—a localized source of stress—is the only scenario that can account for the distinct stress state. The total stress tensor in the ETSZ would be the sum of the regional compressional stress field manifest in most CEUS earthquakes and this local stressor, plus any other smaller-scale stress perturbations. Notably, the presence of a local source of stress need not elevate earthquake rates. Rather, the total strain rate tensor is governed by the deviatoric component of this summed stress tensor, so if the local and regional stress fields do not interfere constructively, overall strain rate would be anticipated to decrease.

The extent to which the anomalous stress is expected to increase seismicity can be determined by forward modeling the full stress tensor (tectonic stress plus local stressor). If total deviatoric stress in the ETSZ is 5–10 times higher than the CEUS average, then historical seismicity rates are readily explained (in the case of linear viscosity; non-linear rheologies would require less stress elevation). By contrast, if stress magnitudes are similar, then the local stress perturbation that alters the stress state does not account for earthquake rates, and another coincident phenomenon must be active. Earthquake rates are not a constraint on the origin of the stress anomaly. Instead, an explanation that for the stress field will be sought by forward modeling of the impacts of hypothesized local stress, and the degree to which long-term total stress explains historical seismicity rates will be an ancillary result.

4.1. WINNOWING EXISTING HYPOTHESES

The anomalous state of stress in the ETSZ does not uniquely identify the phenomenon responsible, yet myriad variations on the four main classes have been proposed. Those that can be discarded at this point because they do not explain the stress anomaly (though these could elevate earthquake rates) include:

Transients:

Aftershocks following a major—but undocumented—prehistoric event [Ebel, 2008]

Naturally periodic clustering of intraplate moment release [e.g., Clark et al., 2012]

Weakness:

Low-friction/high fluid-pressure faults [e.g., Kauffman and Long, 1996; Steltenpohl et al., 2000]

Low-viscosity mantle [Birjol et al., 2016] or lower crust [Brandmayr et al., 2016]

Reactivation of a (mylonitized?) Proterozoic continental shear zone [Powell and Thomas, 2016]

Exploitation of existing zone of “Concentrated Crustal Deformation” [Thomas and Powell, 2018]

Table 1. Possible causes of ETSZ seismicity that do not explain anomalous stress

The hypotheses left standing invoke a distinct, local source of stress, either dynamic or static in nature:

Stress:

Dynamic response to removal of mantle lithosphere [Birjol et al., 2016]

Dynamic response to removal of negatively buoyant crustal root [Cooley, 2014; Hopper et al., 2016]
 Gravitational stress due to surface loads [Levandowski, 2013; Liu, 2016]
 Gravitational stress due to subsurface density variations [e.g., Grana and Richardson, 1996; Pollitz et al., 2001; Levandowski et al., 2016 for New Madrid and Levandowski et al. 2017 more generally]
 Stress “concentration” at a rheological boundary [Powell et al., 1994; Vlahovic et al., 1998]

Table 2. Possible causes of ETSZ seismicity that do not explain anomalous stress

Clues to winnow down these possibilities, as well as to seek a specific explanation beyond the generalities above, can be deduced from the impact of the local stressor on stress regime and directions, from geologic and tectonic constraints, and from both geophysical data and images.

First, the local stressor does not markedly alter horizontal principal stress directions but instead perturbs the relative magnitude of the vertical stress. Specifically, this perturbation increases vertical (compressive) stress relative to the horizontal stresses. To the east of the ETSZ in South Carolina, ($A\Phi = 2.51$) $\sigma_{\text{ENE-WSW}} > \sigma_{\text{SSE-NNW}} > \sigma_{\text{vertical}}$, and to the north and west ($A\Phi = 1.86$) $\sigma_{\text{ENE-WSW}} > \sigma_{\text{vertical}} \gtrsim \sigma_{\text{SSE-NNW}}$. By contrast, $\sigma_{\text{vertical}} \gtrsim \sigma_{\text{ENE-WSW}} \gg \sigma_{\text{SSE-NNW}}$ in the ETSZ. Therefore, the local stress may be relatively azimuthally isotropic (the horizontal components are roughly equal) compared to the regional field on which it superposes and must be dominated by a vertical component that favors extension, at least at seismogenic depths. (An alternative is that the local stressor has substantial horizontal deviatoric components with orientations indistinguishable from the tectonic field. Regardless, it must be dominated by vertical maximum compression.)

Potential field anomalies whisper a second hint. That the densest concentration of ETSZ seismicity abuts a major magnetic lineament, the NYAL, implies a connection with a lithospheric-scale and continental-scale basement feature. One possibility is that some property of the comparatively non-magnetic basement southeast of the NYAL (e.g., yield strength) focuses strain relative to the magnetic basement northwest of the suture [e.g., Brandmayr et al., 2016]. More importantly, however, Bouguer and isostatic residual gravity lows straddle the NYAL, opening up the possibility that Proterozoic (or subsequent) activity along the suture has altered basement rocks [e.g., Powell et al., 2014]. Setting aside the cause of the evident density anomaly to examine the physics of the situation conceptually, negative isostatic residual gravity (Figure 1B) suggests that topographic disequilibrium could be a factor. Specifically, the isostatic gravity low implies mass deficit relative to surface elevation: Absent flexural strength and in steady state, the ETSZ would be at a higher elevation than at present. Topography may be overcompensated by lithospheric buoyancy (plus any sublithospheric component) and either suppressed—rather than supported—by flexure or not yet in equilibrium.

4.2. THE CASE FOR GRAVITY-DERIVED STRESS

Revisiting the hypotheses listed above in light of these two observations, gravitational effects provide a unifying possibility. Several different flavors of gravity-driven stress changes have been offered in previous work. Seismic tomography and 1D receiver function-type models have respectively been interpreted to portray removal of negatively buoyant mantle lithosphere or lower crust [Biryol et al., 2016; Graw et al., 2015]. Uplift in response to foundering would promote uplift in the overlying material, which creates tension via flexural fiber stress [Levandowski, 2013], increased elevation and therefore gravitational potential energy [e.g., Jones et al., 2004], and the erosion-mediated feedback between the two [Gallen et al., 2018]. The elastic flexural strength of the lithosphere allows a static or quasi-static stress response to buoyancy changes, also prolonged by positive feedback with erosion, so foundering need not be presently active. At their essence, the foundering hypotheses simply invoke lateral density

contrasts that create horizontal gradients in lithostatic pressure. *McGarr* [1988] originally distilled this concept to the idealized case of non-Airy surface topography, and the steeply incised landscapes of Eastern Tennessee necessarily produce several MPa of lateral pressure variations in the shallow crust. Similarly, heterogeneous crust—its magnetic heterogeneity is patent—can be maintained indefinitely by elastic strength, “freezing in” crustal and mantle lithospheric density variations. As explored extensively in New Madrid [*Grana and Richardson*, 1996; *Pollitz et al.*, 2001; *Levandowski et al.*, 2016], *in-situ* density contrasts can create stress sufficient to alter stress regime and directions, and to focus seismicity.

Such *in-situ* density variations are obvious from gravity data, as discussed above. Moreover, the gravity-derived deviatoric stress tensor is dominated by the vertical component and is azimuthally isotropic for simple bodies and rheologies [e.g., *Fleitout and Froidevaux*, 1982], similar to the inferred characteristics of the ETSZ’s local stressor.

Because tectonism may thicken or thin the crust, emplace igneous intrusions, cause metamorphism, or alter lithospheric density in any number of other ways, anomalous densities (in addition to faults) may be expected, rather than surprising, consequences of prior deformation such as the NYAL generally and ETSZ specifically. Similarly, instability can be introduced over time by cooling and (usually pro-grade) metamorphism, especially in orogenic belts [e.g., *Fischer et al.*, 2002].

4.3. STRESS IMPACTS OF INHERITED DENSITY VARIATIONS

Multiple studies have explored the impacts of *ad hoc* or idealized inherited intracrustal density anomalies [*Grana and Richardson*, 1996; *Zoback and Richardson*, 1996; *Pollitz et al.*, 2001]. In the simple case of a single, frozen-in, dense anomaly meant to represent a mafic underplate near New Madrid, *Grana and Richardson* [1996] demonstrated that gravity-derived stress is tensile below the body—where lithostatic pressure is greater than adjacent areas—but is compressive above the body. Over time, the surface above a dense body will subside and fill with low-density sediment, and the lithostatic pressure deficit relative to basin flanks further increases compressive stress. Conversely, buoyant material promotes uplift and therefore tensile stress above [e.g., *Becker et al.*, 2015], and surface uplift creates a shallow pressure excess and reinforces normal faulting [e.g., *Levandowski et al.*, 2017]. Erosion plays a part in tempering this effect (except that it strips the shallowest, generally lowest-density material), but erosion also sets off continued flexural-isostatic uplift and therefore renewed tension [e.g., *Gallen and Thigpen*, 2018].

Idealized simulations or even analytical calculations [*Fleitout and Froidevaux*, 1982; *Artyushkov*, 1973] are valuable for their simplicity and certainty, but in the ETSZ the numerous competing or even complementary hypotheses that invoke or imply density anomalies are better treated with an agnostic approach. Any one of the hypotheses could reproduce observations if the density model is idealized appropriately, so the approach used here will be to develop a 3D density model of the crust and upper mantle from seismic data, heat flow, topography, and gravity data [following *Levandowski et al.*, 2015]. The 3D gravity-derived stress field attendant to this density model is then computed objectively by finite-element simulations. Interpretation of the causes of prominent density anomalies is subjective, based on their spatial distribution, depth range, amplitude, and external constraints [e.g., *Levandowski et al.*, 2018b].

4.4. MODELING GRAVITY-DERIVED AND TECTONIC STRESS

Gravity-derived stress is superimposed on broad stress fields associated with plate interactions and motions. Nevertheless, the magnitude of deviatoric stress(ing) transmitted into continental interiors is known only to be less than the ~100 MPa required for frictional faulting. Also, orientations and relative magnitudes of principal stress are deduced from *in-situ* stress indicators and focal mechanisms, which reflect the total stress field, not just the tectonic component. Therefore, the final procedural step in this analysis is to seek the regional stress field that—when summed with the finite-element modeled gravity-derived stress—best fits focal mechanism inversions (stress directions and relative magnitudes) and *in-situ* horizontal stress direction indicators, mainly borehole breakouts [*World Stress Map: Heidbach et al.*, 2016].

In essence, this approach is a hypothesis test. The implied hypothesis is that the stress field manifest in seismicity and borehole breakouts is primarily the sum of the stress associated with the current 3D density structure of the crust and upper mantle and a single tectonic stress field. Remaining variations comprise the effects of other (implicitly minor) stress sources, uncertainty in the models, or outright failure of the hypothesis. The fit to stress ratios and directions determines the validity of the model, and it is entirely independent of stress(ing) magnitudes. These levels of long-term stress are an ancillary product of the investigation, yet they will illuminate how much of the variability in historical earthquake rates can be ascribed to differences in long-term stress(ing). If the ETSZ experiences 5–10 times the average CEUS deviatoric stress, high seismicity rates are explained and are expected to remain high as long as the causative phenomenon is present. Lower levels of stress imply that one or more additional factor is at play in the ETSZ.

5. LITHOSPHERIC DENSITY

The hypotheses in **Table 2** make testable predictions about crustal and/or mantle structure. Nevertheless, the best-resolved local crustal model [*Powell et al.*, 2014] has no mantle component, the most recent targeted mantle model [*Biryol et al.*, 2016] has no resolution in the crust, and comprehensive lithospheric velocity models derived from Transportable Array data [e.g., *Shen and Ritzwoller*, 2016] have lateral resolution of >70 km. Furthermore, the computation of gravity-derived stress requires a reliable 3D density model. The approach here takes 3D seismic velocity models systematically derived from Transportable Array data, uses gravity data (15 arc-second, ~0.5 km, resolution) to sharpen images, and inverts for a final model at 15-km resolution that reproduces gravity and flexurally modulated topography to within 5 mGal and 50 meters.

The final 3D density model provides a simple means to qualitatively test the hypotheses in Table 2, summarized in Table 3. Beyond this qualitative assessment, however, finite-element models can determine whether the structures associated with these possibilities do, in fact, account for the anomalous extension. Finally, the magnitudes of associated stress quantify the extent to which the anomalous stress in the ETSZ accounts for high seismicity rates.

Hypothesized stressor	Crustal/upper mantle signature
Dynamic response to removal of mantle lithosphere [<i>Biryol et al.</i> , 2016]	Buoyant upper mantle and/or isolated high-density body below lithosphere
Dynamic response to removal of negatively buoyant crustal root [<i>Cooley</i> , 2014; <i>Hopper et al.</i> , 2016]	Buoyant lower crust and/or isolated high-density body below lithosphere
Gravitational stress due to surface loads [<i>Levandowski</i> , 2013; <i>Liu</i> , 2016]	Indistinct, but without sufficient lateral variations at depth to generate appreciable gravity-derived stress

Gravitational stress due to subsurface density variations [e.g., <i>Grana and Richardson, 1996; Pollitz et al., 2001; Levandowski et al., 2016</i> for New Madrid and <i>Levandowski et al. 2017</i> more generally]	Lateral variations at depth generate appreciable gravity-derived stress, specifically buoyant material below seismogenic ETSZ mid-crust, dense material above, or both
Stress “concentration” (refraction) at a rheological boundary [<i>Powell et al., 1994; Vlahovic et al., 1998</i>]	Lateral contrast in lithospheric properties, localized crustal thickening possible, complex stress field possible

Table 3. Possible causes of ETSZ seismicity and testable predictions about lithospheric structure

5.1. METHOD

A comprehensive image of crustal and upper mantle structure is produced following the approach of *Levandowski et al.* [2015; 2016; 2017; 2018b]: Seismic observations constrain an initial 3D density model that is refined by inversion of gravity and topography. The lithospheric-scale (surface to 150 km) V_s model of *Shen and Ritzwoller* [2016]—which is based on joint inversion of ambient noise H/V, ambient and ballistic Rayleigh wave dispersion (8 to 90s), and receiver functions—and uniform scaling relations [*Levandowski et al., 2015; Deng et al., 2017*] provide an initial estimate of 3D density. Parameterizing this starting density model as a 12x12-km grid with 13 layers that increase in thickness from 5 to 50 km over the 0-150 km depth range, the attendant gravity and flexurally modulated topography (using elastic thickness, T_e , from Kirby and Swain, 2009; Lowry and Pérez-Gussinyé, 2011; Watts, 2012)) are modeled. Comparing predictions to observations (observed topography is smoothed with the same T_e model) yields fields of residual gravity and topography that presumably represent deviations of the true density from the initial model. Finally, these residuals are inverted using the random-walk Monte Carlo algorithm of *Levandowski et al.* [2015] until gravity and topography are universally reproduced to 5 mGal and 50 meters. As in multiple previous studies [*Levandowski et al., 2014; 2016; 2017; Deng et al., 2017*], the initial models generally recover topography and long-wavelength gravity features well, and the refinements primarily serve to sharpen images of crustal structure manifest in the gravity field. Uncertainties are appraised across 1,000 independent realizations by switching among the three T_e models, jackknife-resampling the input velocity model, perturbing the velocity-density scaling (these steps impact the starting model), and simply by the random-walk nature of the inversion algorithm (each chain between starting model and posterior has no “memory” from earlier realizations).

5.2. 3D LITHOSPHERIC DENSITY MODEL OF THE SOUTHEASTERN U.S.

The refined lithospheric images (Figure 3) recover many known features, substantiate some recent findings, and show some remarkable signatures of ancient tectonism. Detailed discussion of the model is deferred to a more general manuscript [*Levandowski et al., “A lithospheric density model of the continental United States”, in preparation for JGR. Late 2020 submission anticipated.*], but in the interest of credence to the pertinent features elaborated below, a cursory overview is given here. Because gravity-derived deviatoric stress is independent of the average pressure and thus density at any given depth; it is the magnitude of pressure disequilibria that matters. Therefore, density is discussed relative to the region-wide median at a given depth.

Thick sediments on the Gulf Coast and Mississippi Embayment manifest as low densities from 0–10 km. A handful of isolated, comparatively high-density (average or greater) patches, roughly circular in plan view, coincide with known or suspected Cretaceous intrusions. The recovery of these small features by the unsupervised Monte Carlo underscores the utility of this approach in mapping anomalies at the appropriate depths and locating small-scale features.

Three discontinuous NNE-trending strings of high-density material in the uppermost (0–10 km) and middle crust (10–30 km) stretch from northern Alabama to Ohio. These strings likely represent the mafic material hypothesized by *Keller et al.* [2010] from potential fields data. The southernmost—in northern Alabama, central Tennessee, and southern Kentucky—envelops the Nashville Dome, an intracratonic uplift 50–125 km northwest of the Appalachian foreland fold and thrust belt. Using structural data, isopach mapping, and gravity, *Abolins and Levandowski* [2017] suggested that the Nashville Dome formed by inversion of a pre-existing rift structure between the Ordovician and Cretaceous, most plausibly during the Allegheny Orogeny. At its southern end, the proposed rift segment terminates against the New York-Alabama lineament, and its northern terminus is near the Rough Creek graben. The age of the original rift structure is under investigation, and it is unknown whether this feature was once continuous with other strings and was subsequently offset (dextrally) or formed as an extensional bridge transferring slip from the NYAL to the Rough Creek graben. A more continuous band of high-density upper crust along the western edge of the extended Atlantic margin marks diabase and other mafic intrusions from Jurassic rifting.

Thinner crust (~35 km) along the Atlantic margin manifests as high density in the 30–50 km depth range. The highest densities at this depth are found near New Madrid, marking a long-known mafic underplate or other intrusions [*Ginzburg et al.*, 1983; *Mooney et al.*, 1983]; the impact of the stress associated with this material on New Madrid seismicity has been investigated [*Grana and Richardson*, 1996; *Pollitz et al.*, 2001; *Levandowski et al.*, 2016]. Between these two, a band of thickened, ~50 km, piles up against the eastern side of the Grenville Front (the western edge of 1.3–0.9 Ga deformation associated with the assembly of Rodinia [*Whitmeyer and Karlstrom*, 2007]). This northeast- then north-trending strip of low density notably underlies the high-density shallow material inferred to represent Precambrian rift segments: These also parallel the Grenville Front but appear restricted to its eastern side. The relationship between the opposite-polarity shallow and deep crustal anomalies is unclear. Crustal thickening could have been cogenetic with inversion of rift-bounding faults, melt extraction from already thickened crust during (failed) rifting would leave buoyant residue, leaky transforms along the Grenville Front could have emplaced mafic units independent of pre-existing buoyant lower crust, and so on. It appears that the Elzvir block (eastern Ohio, western Pennsylvania, western West Virginia), which was accreted during Grenville time, does not have the same thick or thickened crust as elsewhere within the Grenville, plausibly documenting pre-existing thickness differences between the Granite-Rhyolite

Upper mantle shows a similar tri-partite pattern to the uppermost and lowermost crust, with generally low density along the Atlantic margin, comparatively higher density west of approximately the Grenville Front (again, not the Appalachian Front), and low density in the Mississippi Embayment. Superimposed on this general pattern are patchy, somewhat circular density lows in central Virginia, along the southern Atlantic coast in South Carolina and Georgia, and a more modest anomaly near New Madrid. The central Virginia anomaly is well known, coincident with slightly elevated seismicity rates (and the 2011 Mineral, VA earthquake), and anomalous Tertiary volcanism in western Virginia [*Mazza et al.*, 2014]. In the Mississippi Embayment, lithospheric thinning has been proposed by numerous authors on the basis of seismic tomography and may be a relict from Cambrian or earlier rifting. The high density of the Grenville Province(s) mantle reinforces the assertion that its constituent blocks were not extensively rifted [e.g., *Powell et al.*, 2014]. Finally, thinning of the mantle lithosphere during Mesozoic rifting, or perhaps absence of a thick root to begin with in the accreted Appalachian

terrane, is represented by the difference between low densities along the eastern seaboard and higher densities west of the Grenville Front, but the cause of the superposed lows along the southern coast is unknown (verification by other, independent means is needed).

5.3. ANOMALOUS DENSITY STRUCTURE IN THE ETSZ

The ETSZ hosts the most buoyant lower crust anywhere in the SEUS (Fig. 3C), with an average density anomaly (relative to the average at the same depth across the study area) exceeding -100 kg/m^3 over the 30–50 km depth range. Overall, the Grenville Front marks the west side of a zone of thickened crust ($\sim 50 \text{ km}$) that manifests as low densities in the 30–50 km range. An elliptical region $\sim 150 \text{ km}$ NW-SE by 300 km NE-SW of uniquely low density overprints this larger feature from northernmost Alabama/Georgia through Eastern Tennessee to southern Kentucky. Whereas the larger band of thickened crust on the east side of the Grenville Front directly underlies the high-density strings of shallow mafic material, the ETSZ anomaly lies east of the highest-density material so is not compensated by comparatively dense shallow mafics.

6. GRAVITY-DERIVED AND TOTAL STRESS IN THE SOUTHEASTERN U.S.

6.1 APPROACH

In the following, it is assumed that the two chief sources of stress are 3D gravity-derived stress and a regional stress field. This assumption is a hypothesis to be tested: The sum of these two tensors is meant to reproduce the stress-state revealed by inversions of focal mechanisms, and the extent to which it does not reveals the minimum influence of other factors. Both the stress-state and gravity-derived tensor are “known”, so the investigation takes the form of an inverse problem in which the unknown “model” portion is the regional stress field that leads to the best fit to the stress-inversion data. Remaining misfits between the documented stress field and predictions logically comprise noise, errors, and other sources of stress not considered. The latter may include strength contrasts [e.g., *Ravat et al.*, 1987], post-glacial adjustments and surface processes [*Calais et al.*, 2010; *Gallen and Thigpen*, 2018], and any other factor that varies over $\sim 1000 \text{ km}$ or less in the CEUS. Longer-wavelength factors not explicitly considered will be lumped into the optimal regional field found from the nominal inversion.

Work proceeds by combining seismic velocity models, gravity, topography, and heat flow with a simulated annealing/random-walk inversion algorithm to generate 1,000 3D density model of the crust and upper mantle (to 150 km depth). These models serve as the input to a quasi-static finite-element simulation of the attendant gravity-derived stress (Figure 4). Then, a Monte Carlo-style forward modeling routine conducts 10,000 trials of various tectonic boundary conditions on the PyLith finite-element model, solving for the net 3D deviatoric stress field. The normalized misfits of modeled and stress directions and stress ratios at seismogenic depths (5–35 km [*Powell et al.*, 2014]) are then calculated.

6.2 BOUNDARY CONDITIONS

In the CEUS, Mid-Atlantic Ridge push and/or asthenospheric drag create overall ENE–WSW compression. The magnitude of the stress transmitted from the plate boundary to the continental interior is unknown, but several approaches have been used to estimate the magnitude of the stress at ridges, including torque balance, transform valley topography, and global modeling. Using a variety of rheologies—linear and non-linear and with a range of viscosities and power-law exponents—and the acceptable ~ 10 – 100 MPa range of stress at the

Ridge, the range of stress transmitted to the SEUS is $\sim 0\text{--}50$ MPa [Levandowski *et al.*, 2016]. Taking a similar approach to that used here, Levandowski *et al.* [2016] found that the optimal fit to stress indicators in a $\sim 1000 \times 1000$ km region centered on New Madrid was achieved when gravity-derived stress was summed with ~ 5 MPa of ENE-WSW directed compression, though the approach taken therein assumed uniaxial compression, a fixed maximal horizontal stress direction (N64E), and planar geometry. Here, a suite of 10,000 combinations of magnitudes of the regional principal stress and orientation of maximal horizontal stress (projected from spherical to Cartesian coordinates) were added to the modeled gravity-derived stress tensors.

6.3 BEST-FITTING MODEL

Misfits were defined by normalizing misfit in $A\phi$ and σ_{Hmax} by the variance of the input data (i.e., $A\phi$ from stress inversions and limited strain-regime data from World Stress Map indicators, and σ_{Hmax} orientations from inversions and SHmax indicators), dividing weight evenly between $A\phi$ and σ_{Hmax} fits, and weighting individual World Stress Map indicators by respective uncertainty. Minimum misfits are attained with nearly uniaxial ENE-WSW compression (best fit with 4.82 MPa of compression oriented $\sim N65E$, as projected to the center of the study area, and 0.08 MPa of orthogonal tension). Larger tectonic stress limits variations in net stress directions and faulting styles, whereas smaller values do not capture the overall homogeneity in stress directions and long-wavelength variations in deformation regimes (Figure 4).

The best-fitting model (Figure 5) is capable of reproducing gross patterns of stress directions and deformation styles. The clockwise rotation of σ_{Hmax} from north to south along the eastern seaboard is a simple result of plate boundary geometry projected into Cartesian coordinates. By contrast, the clockwise rotation of stress near New Madrid and Guy-Greenbrier results from gravity-derived stress, which promotes ESE-WSW contraction. Addition of this tensor to the regional compression also increases $A\phi$, in that it increases horizontal minimum stress relative to vertical stress, causing the anomalous reverse-oblique motion that characterizes New Madrid and contrasts with nearly pure strike-slip faulting in the surrounding areas. The same appears true for portions of Atlantic margin (e.g., from Virginia southward through South Carolina) with WNW-ESE density gradients inherited from Mesozoic rifting, resulting in biaxial contraction observed near Charleston, SC [Chapman *et al.*, 2016]. Extension in the ETSZ is a simple consequence of the buoyancy structure: The NNE-trending zone of low-density lower crust promotes WNW-ESE extension in overlying material, reinforcing tectonic principal stress directions yet significantly altering the dominant style of deformation.

6.4 STRESS(ING) MAGNITUDES

The optimal stress model makes predictions about the overall magnitude of deviatoric stress(ing) in three dimensions, while the optimal stress model determined above is independent of deviatoric stress magnitude. It therefore remains a testable hypothesis that earthquake rates are highest in areas of elevated long-term loading. For example, lateral viscosity variations at scales of hundreds of km do not substantially alter stress directions but can control strain rates to a greater degree than variations in long-term stress [Ghosh *et al.*, 2020]. Additionally, the naturally periodic character of intraplate strain release, presence of suitably oriented fault networks, and incomplete historical records over timescales far shorter than the average recurrence of even comparatively active intraplate faults could defy a relationship between stress(ing) and earthquake rates. In the simplest case of uniform linear viscosity, however, the magnitude of deviatoric stress would be proportional to strain rate. Further, if b-values, stress drops, and the

proportion of elastic strain energy released coseismically are also effectively uniform, earthquake rates should be proportional to strain rates and therefore to deviatoric stress.

Indeed, the correlation between stress magnitudes and historical seismicity is imperfect, yet anomalously high stress is predicted in the ETSZ and near New Madrid (Figure 4B). Here, stress magnitudes are 5–10 times higher than the CEUS (second invariant ~ 10 s of MPa vs. a few MPa). This difference is remarkably similar to the patterns of long-term seismicity rates: Gutenberg-Richter a -values for 0.1×0.1 degree cells in New Madrid and Eastern Tennessee range from 1 to 3, compared to an average below 0.3 in the eastern U.S. and somewhat lower in most of the central U.S. [Petersen, 2014; Mueller, 2018]. Therefore, gravity-derived stress accounts for the long-term seismicity rate differences between the ETSZ (and New Madrid) and the rest of the CEUS, with no need to invoke viscosity variations, non-steady-state effects, or additional stress perturbations.

The proportionality between stress and earthquake rates is imperfect, however, implying that other factors are locally important. Moderate stress is predicted in southeastern Canada and along the Atlantic coast, yet earthquake rates are elevated in much of this region. Using a 2D thin-sheet model, Ghosh *et al.* [2019] coupled global mantle flow tractions and associated laterally varying lithospheric stress with GPE in eastern North America. A uniform viscosity model overpredicts strain rates in much of the continental interior or underpredicts strain rate along the eastern seaboard, and better strain-rate fit is obtained if the viscosity of the accreted Appalachian terranes and extended Atlantic margin is half (5×10^{24} Pa s) that of the craton. Thus, strain rates are indeed controlled to a great degree by viscosity, but these models also find that neither the absolute magnitudes of viscosity nor lateral viscosity contrasts appreciably alter the fit/misfit between predictions and observed stress directions. Opposite to the case of the Atlantic margin, high stress is predicted on the Gulf Coast despite general seismic quiescence. It is plausible that much of the strain in this area is accommodated aseismically, such as by creep of unconsolidated or poorly consolidated sedimentary units.

6.5 NOTE ON THE RELATIONSHIP BETWEEN MODELED AND IN-SITU STRESS

The term “stress” is used imprecisely here, since the actual magnitudes of differential stress in the brittle crust are controlled by fault friction and typically have values of ~ 100 MPa. By contrast, strain will accrue in viscous material at infinitesimal differential stress. Because the brittle and ductile portions of the lithosphere do not decouple over time (e.g., as evidenced globally by xenoliths), however, the long-term strain rate in the crust is governed by the long-term stress(ing) that drives lithospheric deformation as a whole [as argued by Townend and Zoback, 2001]. Therefore, the stress that is modeled represents a long-term boundary condition, albeit applied internally via body forces, and therefore is more appropriately viewed as stressing rate integrated over an arbitrary timescale. (As an aside, for a stress drop of 1 MPa and deviatoric stress of 5 MPa, the timescale for intraplate faults with recurrence of hundreds to a few thousand years is a few thousand or tens of thousands of years, quite similar to the timescale of ductile lithospheric deformation documented in post-glacial rebound.)

7. DISCUSSION

7.1 ANALAGOUS WESTERN U.S. PROTEROZOIC SUTURE ZONES

Buoyancy-driven extension along major ancestral structures has been previously described in two Proterozoic shear/suture zones in the western Great Plains (Colorado and Wyoming, west/central United States), where uncompensated low-density lower crust generates

suture-normal tension and extension in the overlying crust [Levandowski *et al.*, 2017]. There, the favored explanation for low-density lower crust postulated preferential flux of fluids from the dewatering Farallon slab along lithospheric-scale fractures/sutures and resultant hydration-induced retrogression of garnet-bearing lower crustal assemblages.

In addition to the similarities in paleo-tectonic setting between the NYAL and the Western sutures, *in-situ* hydration of the lithosphere may be a shared commonality. Buoyancy calculations [Jones *et al.*, 2015] suggest that the Great Plains as a whole were hydrated by mantle-derived fluids during the Cenozoic, and hydrous mantle xenoliths [e.g., Davis *et al.*, 1996], metasomatized and retrograded lower-crustal xenoliths [Butcher *et al.*, 2018], flexural models [Leonard, 2002], sedimentological observations [McMillen *et al.*, 2002], and sediment backstripping combined with 3D density models similar to those derived here [Levandowski *et al.*, 2018b] indicate that hydration was likely most intense within these shear/suture zones. Although xenoliths are absent in the ETSZ, magnetotelluric evidence [Murphy *et al.*, 2019] suggests cold but hydrated uppermost mantle lithosphere beneath the southern Appalachians, an interpretation also consistent with *Pn* tomography [McDougall *et al.*, 2015]. This hydration, further, may play a part in a positive feedback with small-scale convection that has been suggested as responsible for Miocene topographic rejuvenation in the southern Appalachians. Fluids liberated from mantle material [e.g., the Farallon slab: Biryol *et al.*, 2016; Sigloch *et al.*, 2007] could force convection (while lowering viscosity) and upwelling, potentially hydrating, weakening, and destabilizing thermal lithosphere. Preferential flux of fluids along the presumably comparatively hydraulically conductive fracture network along the NYAL lithospheric-scale suture zone may also focus hydration-induced retrogression of mantle lithosphere and lower crust, further increasing buoyancy and reinforcing uplift. Such time-dependent topography may also focus seismicity [Becker *et al.*, 2015] as the brittle crust adjusts to changing buoyancy and flow in the underlying upper mantle.

The stress perturbation associated with the Western shear zones, however, occurs in a low regional-stress setting—effectively farther from plate-boundary compressive tractions—where ambient deformation is mostly extensional, and extension directions vary. As such, the gravity-derived stress(ing) is the dominant source of stress [Flesch *et al.*, 2000; Levandowski *et al.*, 2017]. In the ETSZ, however, the spatially isolated stressor overprints the regional contractional deformation field, locally overcoming plate tectonic compression. Furthermore, topographic rejuvenation is observed elsewhere in the southern Appalachians [e.g., Liu, 2016], including many quiescent regions. Therefore, the presence of an inherited suture, and any related geodynamic process, beneath the ETSZ alone is insufficient to account for modern seismicity.

The unique structure of the ETSZ inherited from Proterozoic shear geometry may further influence the interplay between upper mantle processes and seismicity. Specifically, the zone of crustal-scale concentrated deformation manifest, for example, in low-velocity crust from the near-surface to mid-crust or deeper [Powell *et al.*, 2014], may provide an efficient set of conduits for mantle-derived fluids. Indeed, the absence of a distinct Moho arrival on receiver functions near the kink in the NYAL has previously been speculated to result from lower crustal serpentinization or other modification [Graw *et al.*, 2015]. The density-decreasing effects of hydration can be most profound in low-temperature lower crust that is firmly in the garnet stability field, where hydration can induce retrogression of garnet-bearing assemblages to amphiboles and micas [Jones *et al.*, 2015; Butcher *et al.*, 2018]. Therefore, the availability of pathways via suture zones between adjacent distinct terranes and/or heavily fractured crust—especially if these inherited fractures now are in a state of deviatoric tension—may control the

degree and lateral extent of buoyancy increase due to hydration [e.g., *Levandowski et al.*, 2018b] and therefore the associated (tensile) stress increase.

These speculated bottom-up effects would be symbiotic with documented anomalous surface processes in the ETSZ. A late-Miocene base-level drop of ~150 meters in the Tennessee River basin triggered the rapid erosion of Paleozoic sedimentary units from a ~70 km by 350 km swath (WNW–ESE by NNE–SSW) [*Gallen and Thigpen*, 2018]. This unloading has a functionally identical effect to increased sub-seismogenic-zone buoyancy: The overlying material has a tendency to increase in elevation and in so doing is put in relative horizontal tension parallel to the short axis of the eroded swath (i.e., in a WNW–ESE direction). Indeed, the zone of most concentrated ETSZ epicenters is ringed by geomorphic knickpoints, testaments to the time-dependence of topography in the region, and quantitative estimates of total long-term stress perturbations based on the volume of eroded material reach a few MPa [*Gallen and Thigpen*, 2018].

7.2 REFINING THE BOUNDARIES OF THE SEISMOTECTONIC ETSZ

Because of the anomalous rates of seismicity within the ETSZ, a uniform background seismicity rate is applied in the calculation of National Seismic Hazard Model seismicity-based background source model. Specifically, if a given 0.1- x 0.1-degree cell has a historical a -value below the average within the ETSZ, then (with a logic-tree weight of 0.2) the long-term source recurrence in this cell is modeled using an a -value equal to the ETSZ average. The impact of this minimum seismicity rate is negligible in areas within 50 km of moderate historical seismicity, but if the boundaries of this minimum-rate zone extend farther east toward Charlotte, NC or southward toward Birmingham, AL or Atlanta, GA, the impact on annualized risk and on building codes may be considerable.

The main motivation of the present work is to understand the geodynamic origin of the ETSZ in order to delineate the region affected by the same long-term processes responsible for elevated earthquake rates in the known ETSZ, and therefore the region in which the ETSZ-average a -value should be applied in consideration of long-term sources. The thesis of this work is that the ETSZ is an area of elevated long-term deviatoric tension, which is primarily the result of anomalously buoyant lower crust. Therefore, the boundaries of the ETSZ as a hazard entity are defined by the region of net horizontal tension and appreciably elevated stress. For example, although the Giles County Seismic Zone lies within the area of modeled elevated stress, focal mechanisms show strike-slip faulting with secondary contraction. And although seismicity in west-central Alabama is characterized by normal faulting, these earthquakes do not occur in the area of elevated mid-crustal stress; rather than being associated with anomalously buoyant lower crust, these events collocate with exceptionally dense shallow material. (Additionally, hypocenters of these events are mostly shallow—moment tensor solutions are between 3-8 km—compared to the mid-crustal events of the ETSZ [*C.A. Powell, written comm.*, 2019].) The primary difference between the geodynamic and historic-epicentral ETSZ is that the area of modeled elevated tensile stress is more equant than the epicentral distribution, reaching approximately 50 km farther west and 100 km farther east. The impacts of potential changes in zonation must be fully propagated through the National Seismic Hazard Model logic tree, but the results are speculatively minor. The ETSZ does not reach far enough west to impact Nashville, TN or far enough east to impinge on Charlotte, NC. Modest increases in hazard may be considered for intermediate metropolitan areas such as Murfreesboro, TN to the west and Spartanburg/Greenville, SC.

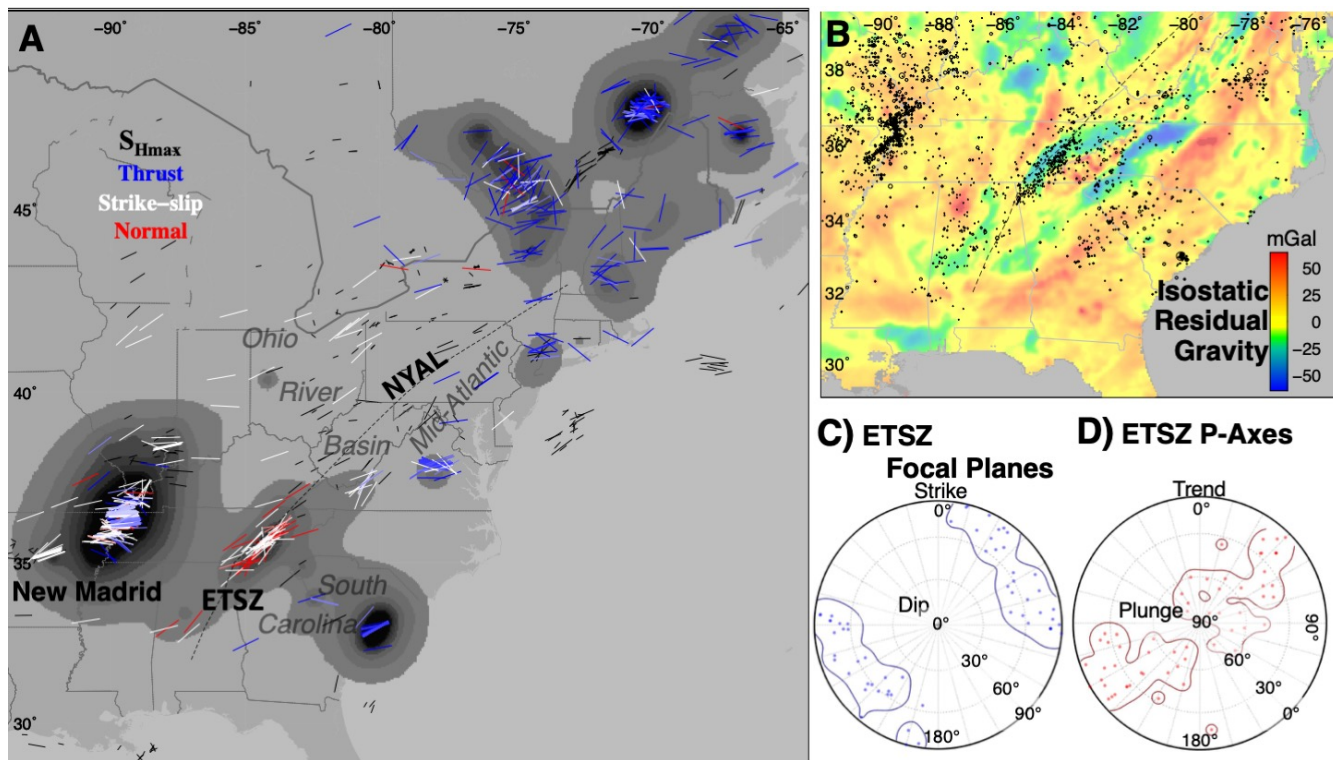


Figure 1. **A)** Maximal horizontal shortening directions of focal mechanisms, colored by faulting style. *In-situ* stress indicators [compiled by *Heidbach et al.*, 2016] shown in black. Darker background shading represents higher seismic hazard. Areas discussed in the text are labeled. ETSZ: Eastern Tennessee Seismic Zone. NYAL: Approximate trace of the New York-Alabama Lineament. **B)** Isostatic residual gravity and seismicity ($M \geq 2.5$). **C)** Stereonet of ETSZ focal plane strike and dip. **D)** Stereonet of ETSZ P-axis trends and plunges.

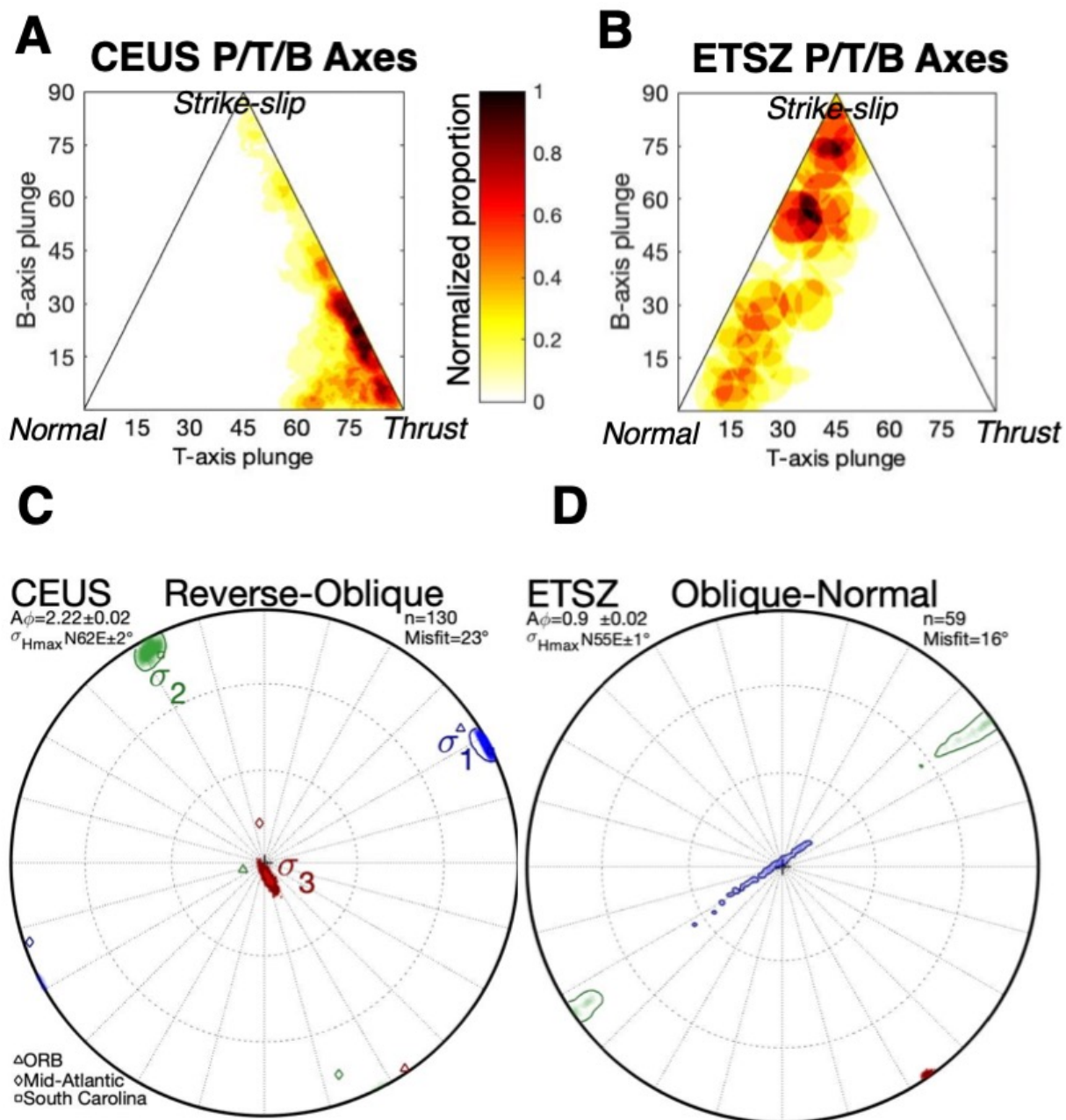


Figure 2. A,B) Ternary contour plot of faulting style [after *Frohlich*, 1992] based on principal axis plunges. The CEUS experiences mainly thrust-type events, with secondary strike-slip faulting. The ETSZ is characterized by deformation along the continuum between normal faulting and strike-slip. **C)** Results of 1000 stress inversions in the CEUS. Median principal axes for constituent subregions are also shown: Ohio River Basin (triangles), South Carolina and surroundings (squares), and the Mid-Atlantic (diamonds). **D)** Results of 100 stress inversions in the ETSZ.

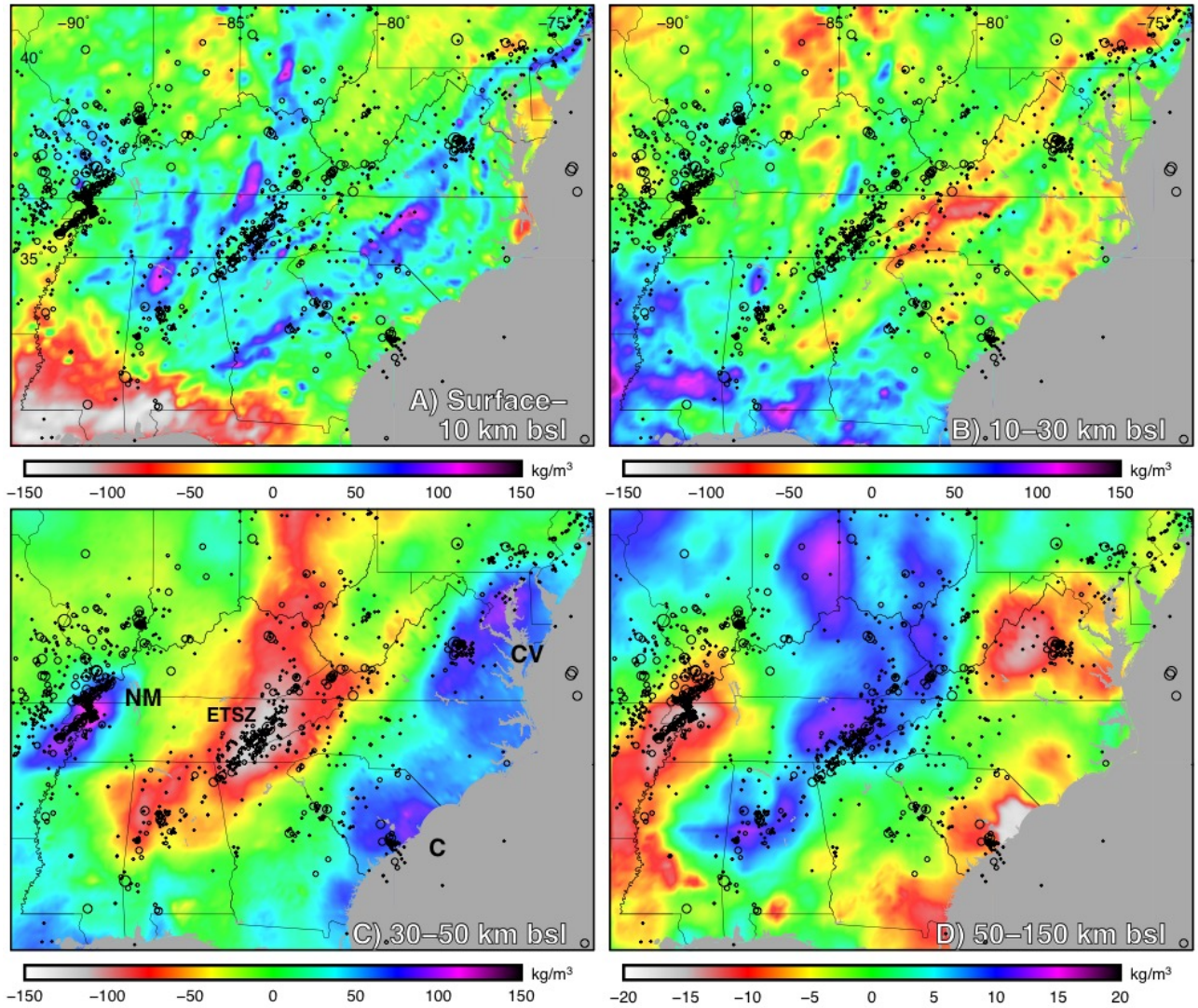


Figure 3: Lithospheric density in the SEUS. The mean density in each layer is removed to facilitate comparison. Earthquakes are from USGS ComCat, hypocenters relocated using a Bayesian algorithm [Will Yeck, USGS, written comm. 2016]. The four main SEUS seismic zones collocate with anomalous crust and/or upper mantle. Reverse to reverse-oblique motion in New Madrid (NM), Central Virginia (CV), and Charleston (C) occurs above variably dense lower crust and buoyant upper mantle. By contrast, ETSZ oblique-normal faulting occurs above the most buoyant lower crust anywhere in the SEUS.

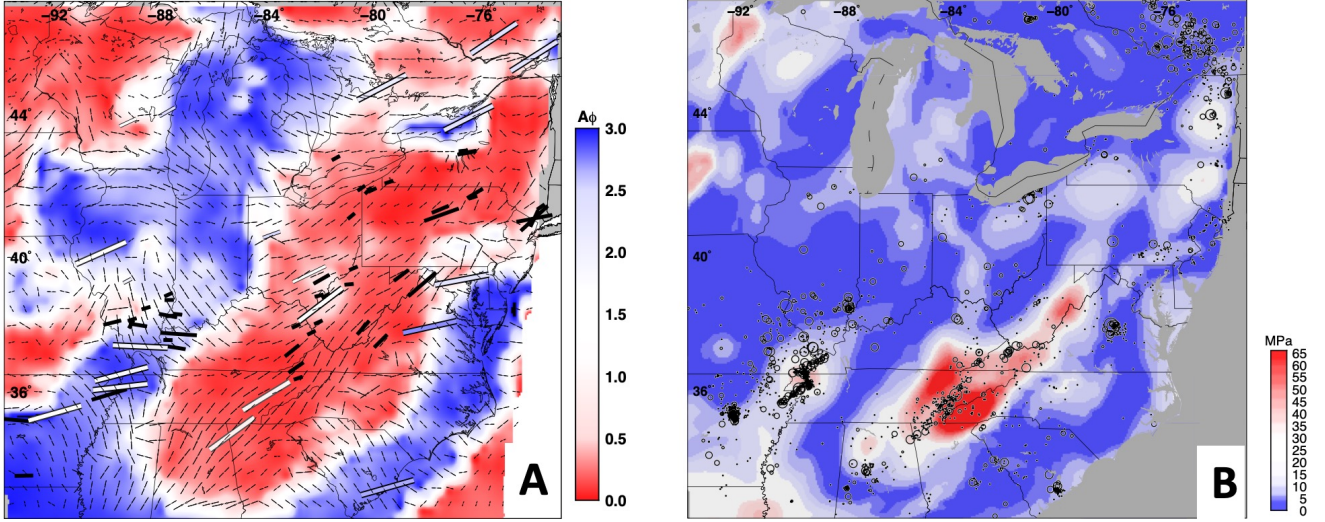


Figure 4. Stress due to density variations alone.

A) Stress direction and strain regime. Bold arrows: World Stress Map SHmax indicators, scaled by quality [Heidbach *et al.*, 2016]. Colored bars: Stress inversion results. Oriented to σ_{Hmax} and colored by $A\phi$. Thin arrows: Predicted σ_{Hmax} . Background colored by predicted $A\phi$. Predictions (thin arrows and background color) depict the average values between 5 and 30 km depth, similar to seismogenic depths in the ETSZ. Discussion is deferred to the total stress model.

B) Stress magnitude quantified as the second invariant of the deviatoric stress tensor. Discussion is deferred to the total stress model.

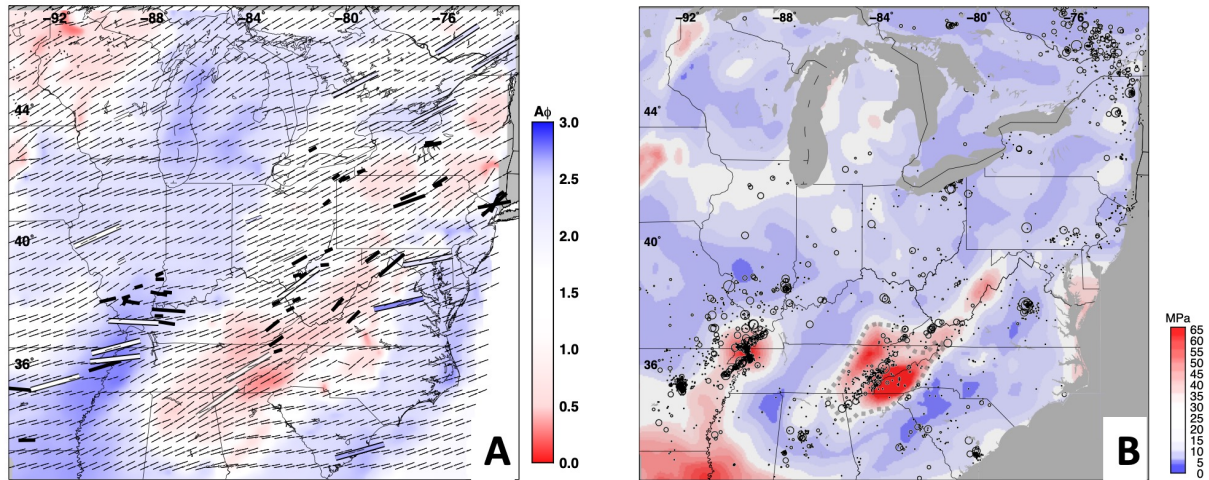


Figure 5.

A) Stress direction and strain regime. Bold arrows: World Stress Map SHmax indicators, scaled by quality [Heidbach *et al.*, 2016]. Colored bars: Stress inversion results. Oriented to σ_{Hmax} and colored by $A\phi$. Thin arrows: Predicted σ_{Hmax} . Background colored by predicted $A\phi$. Predictions (thin arrows and background color) depict the average values between 5 and 30 km depth, similar to seismogenic depths in the ETSZ.

B) Stress magnitude, quantified as the second invariant of the deviatoric stress tensor. New Madrid, the ETSZ, and the Gulf Coast are predicted to experience the greatest deviatoric stress. The 5- to 10-fold difference between the ETSZ and average CEUS is approximately proportional to the difference in earthquake rates, suggesting that long-term stress alone may account for ETSZ activity. A polygon showing the proposed delineation of the ETSZ as a geodynamic and seismotectonic entity is shown as a dotted gray line.

Data Access

Gravity and topography data were provided by https://topex.ucsd.edu/cgi-bin/get_data.cgi

Moment tensor solutions from

http://www.eas.slu.edu/eqc/eqc_mt/MECH.NA/MECHFIG/mech.html

Other focal mechanisms from references given in text.

In-situ stress indicators from <http://www.world-stress-map.org>

Seismic velocity models from *Shen and Ritzwoller* (2016, *JGR*).

Density inversion code from Levandowski et al. (2015, *Geochemistry, Geophysics, Geosystems*), available from the author by request.

REFERENCES

- Angelier, J. (1979). Determination of the mean principal directions of stresses for a given fault population, *Tectonophysics* 56.
- Artyushkov, E. V. (1973). Stresses in the lithosphere caused by crustal thickness inhomogeneities. *Journal of Geophysical Research*, 78(32), 7675-7708.
- Becker, T. W., Lowry, A. R., Faccenna, C., Schmandt, B., Borsa, A., & Yu, C. (2015). Western US intermountain seismicity caused by changes in upper mantle flow. *Nature*, 524(7566), 458-461.
- Bockholt, B. M., Langston, C. A., & Withers, M. (2015). Local magnitude and anomalous amplitude distance decay in the eastern Tennessee seismic zone. *SRL*, 86(3).
- Bockholt, B.M. (2014). A seismogenic study of the central and eastern United States, Doctoral Dissertation, University of Memphis, Memphis Tennessee, 153 pp.
- Bollinger, G. A. (1973). Seismicity of the southeastern United States, *BSSA*, 63(5).
- Biryol, C. B., Wagner, L. S., Fischer, K. M., & Hawman, R. B. (2016) Relationship between observed upper mantle structures and recent tectonic activity across the Southeastern United States, *JGR* 121.
- Blackwell, David, M. Richards, Z. Frone, J. Batir, A. Ruzo, R. Dingwall, and M. Williams 2011, Temperature at depth maps for the conterminous US and geothermal resource estimates, *GRC Transactions*, 35 (GRC1029452).
- Brandmayr, E., & Vlahovic, G. (2016) The upper crust of the Eastern Tennessee Seismic Zone: Insights from potential fields inversion, *Tectonophysics*, 685.
- Butcher et al., 2018
- Chapman, M. C., C. A. Powell, G. Vlahovic, and M. S. Sibol (1997), The nature of faulting in eastern Tennessee inferred from a statistical analysis of focal mechanisms and epicenter locations, *BSSA*, 87.
- Clark, D., A. McPherson, and R. Van Dissen (2012), Long-term behaviour of Australian stable continental region (SCR) faults, *Tectonophysics*, 566.
- Cooley, M. T. (2014) New set of focal mechanisms and geodynamic model for the Eastern Tennessee Seismic Zone, M.S. Thesis, University of Memphis.
- Crone, A. J., Machette, M. N., and Bowman, J. R. (1997), Episodic nature of earthquake activity in stable continental regions revealed by palaeoseismicity studies of Australian and North American quaternary faults, *Aus. JES*, 44.
- D'Agrella-Filho, M.S., Tohver, E., Santos, J.O.S., Elming, S.-A., Trindade, R.I.F., Pacca, I.I.G., and Geraldies, M.C., 2008, Direct dating of paleomagnetic results from Precambrian sediments in the Amazon craton: Evidence for Grenvillian emplacement of exotic crust in SE Appalachians of North America, *EPSL*, 267.

- Ebel, J. E., Bonjer, K. P., & Oncescu, M. C. (2000). Paleoseismicity: Seismicity evidence for past large earthquakes, *SRL*, 71(2).
- Ebel, J. E. (2008) The importance of small earthquakes, *SRL*, 79(4).
- Fleitout, L., & Froidevaux, C. (1982). Tectonics and topography for a lithosphere containing density heterogeneities. *Tectonics*, 1(1), 21-56.
- Flesch, L. M., Holt, W. E., Haines, A. J., & Shen-Tu, B. (2000). Dynamics of the Pacific-North American plate boundary in the western United States. *Science*, 287(5454), 834-836.
- Gallen, S. F., & Thigpen, J. R. (2018). Lithologic controls on focused erosion and intraplate earthquakes in the eastern Tennessee seismic zone. *Geophysical Research Letters*, 45(18), 9569-9578.
- Ghosh, A., Holt, W. E., & Bahadori, A. (2019). Role of large-scale tectonic forces in intraplate earthquakes of Central and Eastern North America. *Geochemistry, Geophysics, Geosystems*, 20(4), 2134-2156.
- Grana, J. P., & Richardson, R. M. (1996). Tectonic stress within the New Madrid seismic zone. *Journal of Geophysical Research: Solid Earth*, 101(B3), 5445-5458.
- Graw, J.H., C.A. Powell, and C.A. Langston (2015), Crustal and upper mantle velocity structure in the vicinity of the eastern Tennessee seismic zone based upon radial P-wave transfer functions, *JGR*, 120.
- Hardebeck, J. L. (2012). Coseismic and postseismic stress rotations due to great subduction zone earthquakes. *Geophysical Research Letters*, 39 (21).
- Heidbach, O., Rajabi, M., Reiter, K., Ziegler, M., & Wsm Team. (2016). World stress map database release 2016. *GFZ Data Services*, 10.
- Herrmann, 2019 http://www.eas.slu.edu/eqc/eqc_mt/MECH.NA/MECHFIG/mech.html. Accessed 06/30/2019.
- Herrmann, R. B., Malagnini, L. & Munafó, I. Regional moment tensors of the 2009 L'Aquila earthquake sequence. *Bull. Seismol. Soc. Am.* 101, 975–993 (2011).
- Hurd, O., & Zoback, M. D. (2012). Intraplate earthquakes, regional stress and fault mechanics in the Central and Eastern US and Southeastern Canada. *Tectonophysics*, 581, 182-192.
- Hurd, O., & Zoback, M. D. (2012). Regional stress orientations and slip compatibility of earthquake focal planes in the New Madrid seismic zone. *Seismological Research Letters*, 83(4), 672-679.
- King, E. R., and Zietz, I., 1978, The New York-Alabama lineament: Geophysical evidence for a major crustal crustal break in the basement beneath the Appalachian basin, *Geology*, v. 6, p. 312-318.
- Jones, C. H., Mahan, K. H., Butcher, L. A., Levandowski, W. B., & Farmer, G. L. (2015). Continental uplift through crustal hydration. *Geology*, 43(4), 355-358.
- Levandowski, W., & Powell, C. A. (2019). Evidence for strain accrual in the Eastern Tennessee Seismic Zone from earthquake statistics. *Seismological Research Letters*, 90(1), 446-451.
- Levandowski, W., Herrmann, R.B., Briggs, R., Boyd, O.S., and Gold, R. (2018) An updated stress map of the continental United States reveals heterogeneous intraplate stress: *Nature Geoscience*. doi:10.1038/s41561-018-0120-x.
- Levandowski, W., Boyd, O. S., Briggs, R. W., & Gold, R. D. (2015). A random-walk algorithm for modeling lithospheric density and the role of body forces in the evolution of the Midcontinent Rift. *Geochemistry, Geophysics, Geosystems*, 16(12), 4084-4107.
- Levandowski, W., Zellman, M., and Briggs, R. (2017) Gravitational body forces focus North American intraplate earthquakes, *Nature Comm.*, 8(14314).

Levandowski and Jones, 2018

- Liu, L. (2016) Rejuvenation of Appalachian topography by subsidence-induced differential erosion, *Nat Geo*, 7.
- Mazza, S. E., Gazel, E., Johnson, E. A., Kunk, M. J., McAleer, R., Spotila, J. A., ... & Coleman, D. S. (2014). Volcanoes of the passive margin: The youngest magmatic event in eastern North America. *Geology*, 42(6), 483-486.
- Mazzotti, S., & Townend, J. (2010). State of stress in central and eastern North American seismic zones. *Lithosphere*, 2(2), 76-83.
- McGarr, A. (1988) On the state of lithospheric stress in the absence of applied tectonic forces. *JGR*, 93.
- McKenzie, D. P. (1969). Speculations on the consequences and causes of plate motions. *Geophysical Journal International*, 18(1), 1-32.
- Murphy, B. S., & Egbert, G. D. (2019). Synthesizing seemingly contradictory seismic and magnetotelluric observations in the southeastern United States to image physical properties of the lithosphere. *Geochemistry, Geophysics, Geosystems*, 20(6), 2606-2625.
- Montagner, J. P., and D. L. Anderson (1989), Petrological constraints on seismic anisotropy, *PEPI*, 54.
- Moschetti, M. P., M. H. Ritzwoller, F. Lin, and Y. Yang (2010), Seismic evidence for widespread western U.S. deep crustal deformation caused by extension, *Nature*, 464, 885–889, doi:10.1038/nature08951.
- Petersen, M.D. *et al.* (2008). Documentation for the 2008 Update of the United States National Seismic Hazard Maps: USGS Open File Report 2014-1128.
- Petersen, M.D. *et al.* (2014). Documentation for the 2014 Update of the United States National Seismic Hazard Maps: USGS Open File Report 2014-1091.
- Pollitz, F. F., and W. D. Mooney (2016), Seismic velocity structure of the crust and shallow mantle of the Central and Eastern United States by seismic surface-wave imaging, *GRL*, 43.
- Powell, C. A., G. A. Bollinger, M. C. Chapman, M. S. Sibol, A. C. Johnson, and R. L. Wheeler (1994), A seismotectonic model for the 300 kilometer long eastern Tennessee seismic zone, *Science*, 264.
- Powell, C. A., Withers, M., Cox, R. T., Vlahovic, G., and Arroucau, P. (2014) Crustal velocity structure associated with the eastern Tennessee seismic zone: Vp and Vs images based upon local earthquake tomography, *JGR*, 119.
- Powell, C.A., and W.A. Thomas (2016), Grenville basement structure associated with the eastern Tennessee seismic zone, southeastern USA, *Geology*, v.44, 39-42, doi:10.1130/G37269.1.
- Sbar, M. L., & Sykes, L. R. (1973). Contemporary compressive stress and seismicity in eastern North America: An example of intra-plate tectonics. *Geological Society of America Bulletin*, 84(6), 1861-1882.
- Shen, W. and Ritzwoller, M.H. (2016) Crustal and upper mantle structure beneath the United States, *JGR*, 121.
- Stein, S., Liu, M., 2009. Long aftershock sequences within continents and implications for earthquake hazard assessment. *Nature*, 462.
- Steltenpohl, M. G., Zietz, I., Horton Jr., J. W., and Daniels, D. L., 2010, New York– Alabama lineament: A buried right-slip fault bordering the Appalachians and mid-continent North America: *Geology*, 38(6).

- USGS, 2019. <https://earthquake.usgs.gov/earthquakes/search/> Accessed 06/30/2019.
- Vavručuk, V. (2014) Iterative joint inversion for stress and fault orientations from focal mechanisms, GJI, 199.
- Wagner, L.S., Long, M.D., Johnston, M.D., and Benoit, M.H., 2012, Lithospheric and asthenospheric contributions to shear-wave splitting observations in the southeastern United States, EPSL, 341-344.
- Whitmeyer, S. J., & Karlstrom, K. E. (2007). Tectonic model for the Proterozoic growth of North America. *Geosphere*, 3(4), 220-259.
- Zoback, M. L., and Zoback, M. D. (1980). State of stress in the conterminous United States. JGR, 85.

Results for random vs. optimal planes

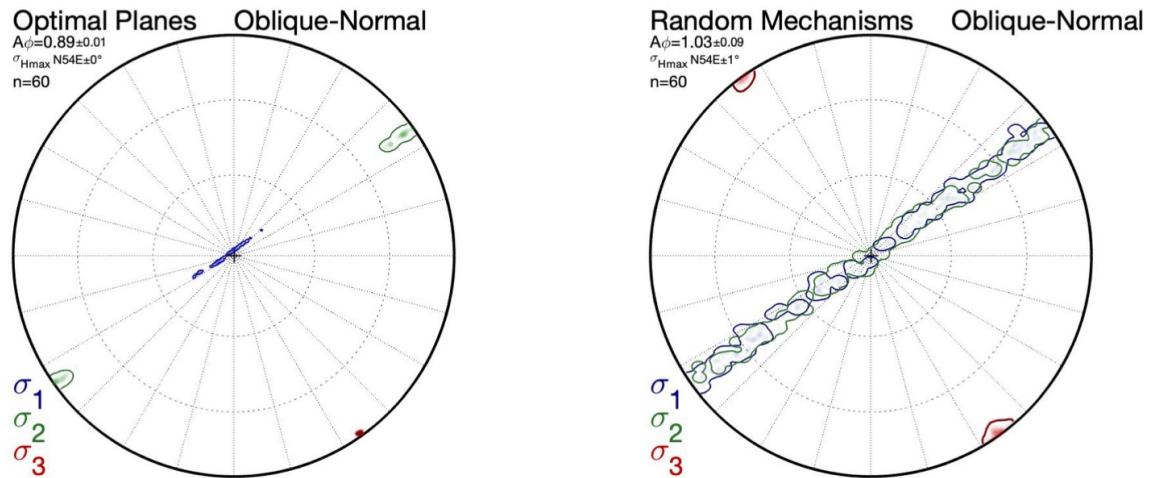


Figure S1. Comparison of stress inversion results using best-fitting focal mechanisms ("Optimal Planes") and randomly selected mechanisms. Optimal planes lead to essentially the same result but have greater precision.

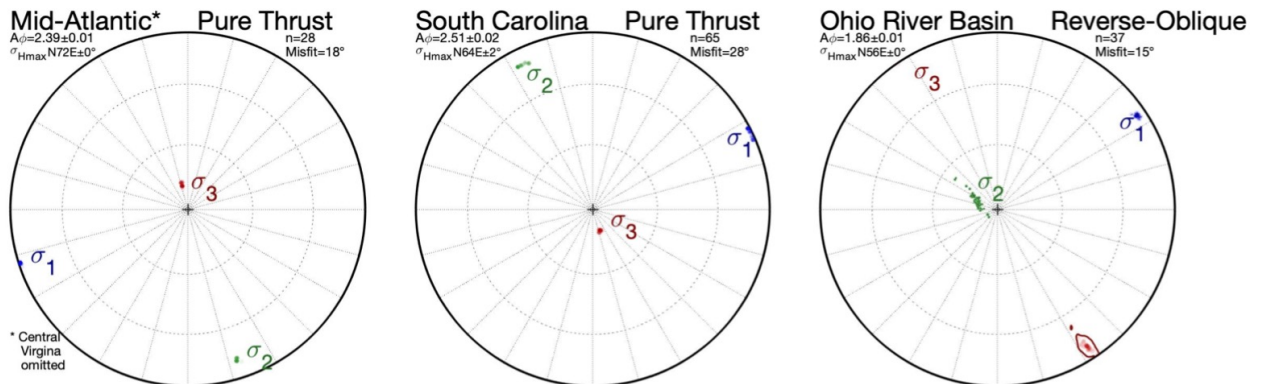


Figure S2: Stress inversions for seismic zones surrounding the ETSZ.

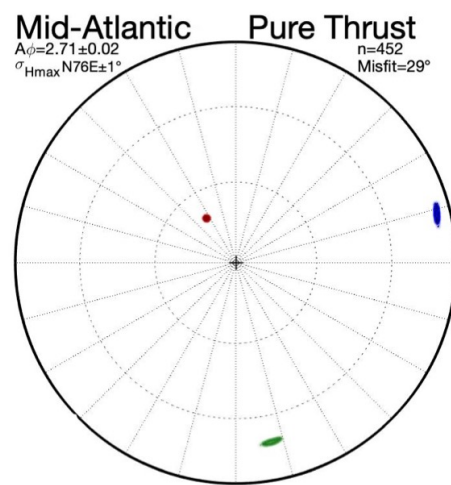


Figure S3: Mid-Atlantic inversion, including central Virginia events.